Determination of Ductile Material Properties by Means of the Small Punch Test and Neural Networks

Martin Abendroth*, Meinhard Kuna
Technische Universität Bergakademie Freiberg
Institute of Mechanics and Fluid Dynamics
Lampadiusstraße 4, D-09596 Freiberg, Germany

July 13, 2004

Abstract

This paper compares two different methods for the identification of ductile properties of materials. Both methods use the small punch test to measure the material response under loading. The resulting load displacement curve contains information about the deformation behavior of the tested material. The finite element method is used to calculate the load displacement curve of the punch depending on the parameters of a material law. Via a systematical variation of the material parameters a data base is built up, which is used to train neural networks. This networks can be used either as an inverse function for the determination of material parameters from a measured load displacement curve or as a function approximating directly the finite element solution. The second method allows the indentification of material parameters by using a conjugate directions algorithm, which minimizes the error between an experimental load displacement curve and one calculated by the network function. Both methods are described in detail and results are discussed.

Keywords: small punch test, neural networks, ductile materials, finite elements, parameter identification

1 Introduction

The ductile material behavior in structural components is changing due to in service loading, aging, irradiation, embrittlement a.o., which requires an in situ monitoring of the material state. In order to determine material parameters at various locations e.g. in weldments or gradient materials, the

*email: Martin.Abendroth@imfd.tu-freiberg.de

size of the material taken out for a test specimen should be very small but representative.

In the small punch test (SPT), a disk like specimen of $\varnothing 8 \times 0.5\,\mathrm{mm}$ size is deformed in a miniaturized deep drawing experiment. The measurable output is the load displacement curve (LDC) of the punch, which contains information about the elasto-plastic deformation behavior and about the strength properties of the material.

The SPT was introduced to determine post irradiation mechanical properties of materials used in the nuclear industries [1, 2, 3]. Baik et. al. [4] defined the area under the LDC as small punch fracture energy and found correlations between results from Charpy-V-notch and small punch experiments determining the ductile to brittle transition temperature. Some researchers used the SPT to predict the elastic plastic properties [5, 6] and the ductile fracture toughness J_{Ic} [7, 8] or the brittle fracture toughness K_{Ic} [9].

Huber et. al. [10] showed that neural networks (NN) are suitable for the determination of constitutive properties from spherical indentation tests. In [11, 12] deformation and ductile damage properties are determined by using NNs as inverse approximations of the finite element (FE) solution of the SPT.

In the present paper, two different approaches are tested to identify the material parameters of ductile hardening. In both cases the LDC is transfered to a NN, which has been trained with a data base of LDCs generated by FE simulations of the SPT with systematically varied hardening parameters. The NN can either approximate the FE solution directly and the parameter identification is done by a conjugate directions root finding algorithm (case II) or the NN approximates the inverse problem of the FE solution and gives the material parameter as answer directly (case I).

These identification procedures were performed for the materials StE-690, 18Ch2MFA and GGG-40 that are widely used in mechanical engineering. The advantages and restrictions for using both approaches are discussed.

2 Experimental Methods

The SPT is performed using the device as seen in Fig. 1. The specimen (8) is clamped between die (9) and down-holder (4), which are supported by the bottom housing part (7). The screwable upper housing part (3) is used to provide the clamping force. The punch (2) driven by the cross head punch (1) of the testing machine deforms the specimen centrically. The punch displacement is measured (5) parallel to the punch and close to the specimen to prevent errors due to the bending of the cross head of the testing machine and other elastic deformations of the experimental setup. A load

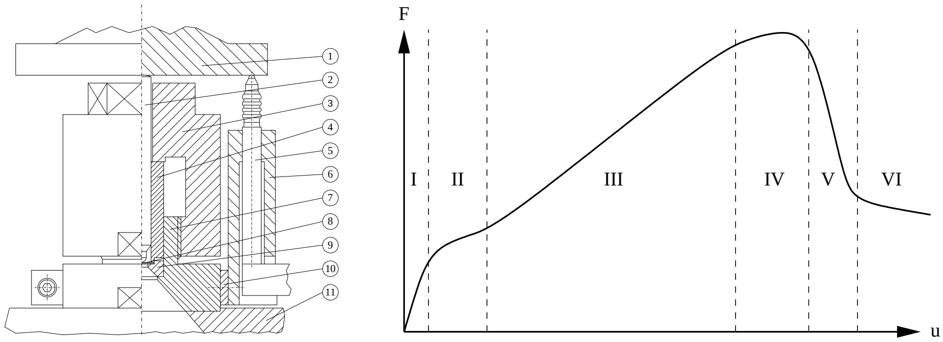

Figure 1: Cross-section of the loading device and the resulting LDC

cell between cross head and punch measures the force acting on the punch.

The result of this experiment is the LDC of the punch, which can be split up into several parts. Part I is mainly determined by the elastic properties of the material, Part II reflects the transition between the elastic and plastic behavior, Part III shows the hardening properties up to part IV where geometrical softening and damage occurs. During the steep decent in Part V the specimen fails and a crack grows circular around the center of the specimen. The remaining force in Part VI is needed to push the punch trough the already cracked specimen.

In order to verify the material parameters determined by the SPT, tensile tests with round notched specimens (see Fig. 2) were carried out additionally. A special video extensometer was used to determine the true stress strain curve. This video extensometer is able to measure the strain in both length and cross direction. Furthermore, the radius of curvature on the necking notch ground was measured to account for the influence of triaxiality using the Bridgman [13] formula. The tensile tests were performed with specimens of the materials 18Ch2MFA and StE-690 only.

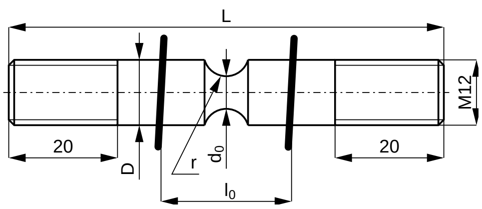

Figure 2: Notched tensile specimen with marks for strain measure

3 Numerical Simulations

After extensive preliminary investigations, a finite element model shown in Figure 3 was developed, which delivers the necessary accuracy by reasonable calculation costs. Since the geometries and the load of the SPT are axisymmetric, a two dimensional finite element model is sufficient. The mesh contains 40×5 axisymmetric reduced integration elements, whereby all elements have a size of 0.1×0.1 mm. The die, down-holder and punch are modelled as rigid bodies. Since the curvature of the punch and the die have a significant influence on the LDC, they have to be modelled very carefully. That's why the exact geometries of these parts have been measured and utilized. Die and down-holder are fixed in all degrees of freedom, whereas the punch can be moved vertically by a displacement boundary condition. The contact between specimen and punch, die and down-holder is modelled including friction with a friction coefficient $\mu = 0.12$.

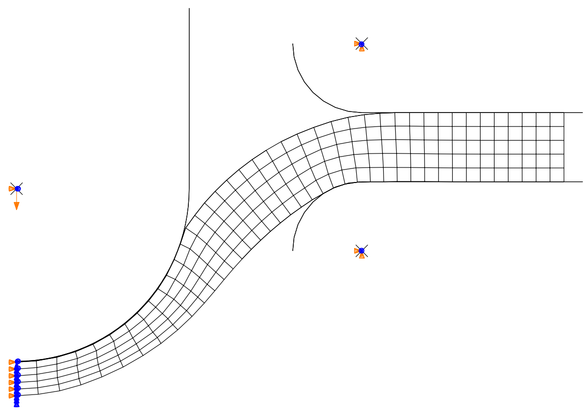

Figure 3: Finite element model of the SPT

3.1 Material model

The material model is based on the constitutive damage law developed by Gurson, Tveergard and Needleman (GTN) [14, 15]. This model assumes an elastic plastic continuum with spherical voids which are allowed to grow only ($f_N = 0$, $f_c = f_f = 1$) in the present analysis. The void volume fraction f is used as a measure of damage. The central part of the model is the yield function

$$\Phi = \left[\frac{\Sigma_V}{\sigma_F(\varepsilon_{pl})}\right]^2 + 2q_1 f \cosh\left[\frac{3}{2}q_2\frac{\Sigma_H}{\sigma_F(\varepsilon_{pl})}\right] - (1 + q_3 f^2) = 0 \qquad (1)$$

where $\Sigma_V = \sqrt{\frac{3}{2}\Sigma'_{ij}\Sigma'_{ij}}$ denotes the v. Mises stress and $\Sigma_H = \frac{1}{3}\Sigma_{kk}$ the hydrostatic stress, expressed by the macroscopic (deviatoric) stresses Σ_{ij} (Σ'_{ij}). The parameters $q_1 = 1.5$, $q_2 = 1$ and $q_3 = q_1^2$ weight the different terms of the yield function. A detailed description of this model and the implementation into the FE-code Abaqus can be found in [16]. In our cases the initial void volume fraction f_0 was determined by the chemical composition of the material. The percentage of carbon in GGG-40 is manifested as small spherical inclusions which can be considered as voids. For steels f_0 can be estimated by the amount of sulfur and manganese that induce non-metallic inclusions [17].

The isotropic hardening behavior of the matrix material is denoted with $\sigma_F(\varepsilon_{pl})$. Three different hardening models (a, b and c) have been taken into consideration. Above the initial yield stress R_e, σ_F is a function of the plastic strain ε_{pl} with the parameters R_e, ε^* and n.

$$\sigma_F(\varepsilon_{pl}) = R_e \left[\frac{\varepsilon_{pl}}{\varepsilon^*} + 1\right]^{\frac{1}{n}} \quad \text{with} \quad \varepsilon^* = \frac{\varepsilon^*_{pl}}{\left[\frac{\sigma^*}{R_e}\right]^n - 1} \tag{2}$$

where $\varepsilon^*_{pl} = 1$ and $\sigma^* = \sigma_F(\varepsilon^*_{pl})$ (model a).

Another possibility (model b) is a description of a true stress strain curve that starts with a perfectly plastic model up to a plastic strain ε_{py}

$$\sigma_F(\varepsilon_{pl}) = \begin{cases} R_e & \text{for} \quad \varepsilon_{pl} < \varepsilon_{py} \\ \sigma^* \varepsilon_{pl}^{1/n} & \text{for} \quad \varepsilon_{pl} \geq \varepsilon_{py} \end{cases}, \tag{3}$$

where ε_{py} depends on R_e and σ^*

$$\varepsilon_{py} = \left(\frac{R_e}{\sigma^*}\right)^n \tag{4}$$

or ε_{py} is an additional plastic strain parameter, beyond of which hardening occurs (model c).

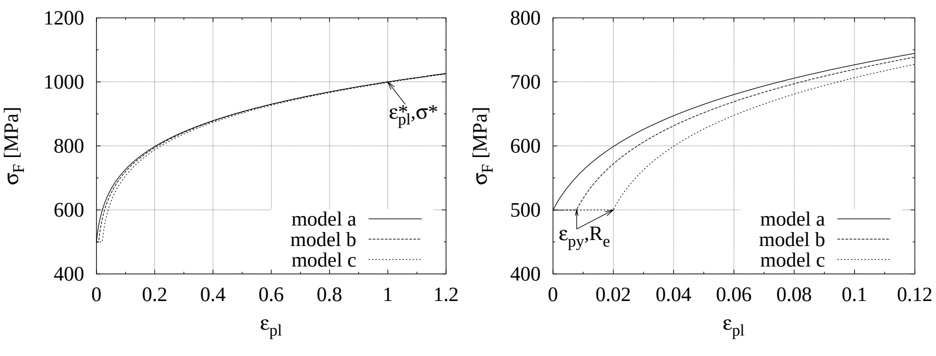

Figure 4: $\sigma_F(\varepsilon_{pl})$-curves R_e =500 MPa, σ^* =1000 MPa, $n = 7$, ($\varepsilon_{py} = 0.02$)

3.2 Building the data bases

To build the LDC data bases for the different hardening models, the parameters have been varied in several steps in ranges as shown in Tab. 1. The data bases contain $11^3 = 1331$ LDCs for model a and b and $6^4 = 1296$ for model c.

	model a			model b			model c		
parameter	min	max	steps	min	max	steps	min	max	steps
σ^* [MPa]	800	1300	11	500	1200	11	500	1200	6
R_e [MPa]	200	700	11	$0.2\sigma^*$	$0.7\sigma^*$	11	$0.2\sigma^*$	$0.7\sigma^*$	6
n	5	15	11	5	15	11	4	14	6
ε_{py}	-	-	-	$\varepsilon_{py} = (R_e/\sigma^*)^n$			0	0.02	6

Table 1: Parameters for building the data bases for the different material models

4 Parameter Identification

To identify the parameters of the true stress strain curve out of the LDC of the SPT two different approaches have been tested. Further on the parameters will be denoted with par_i. The LDC of the SPT is a function for the punch force F depending on the displacement of the punch u and the material parameters par_i.

$$F(u) = f(par_i) \tag{5}$$

To determine par_i two principle ways are possible.

Case I: One can try to find the unknown inverse function $par_i = \varphi(F(u))$ (see Fig. 5). Therefore, the direct problem is solved via FEM. The simulated LDCs are used as input of a NN, to find the material parameters as output. A training algorithm minimizes the error between the answer of the NN par_i' for a computed LDC and its corresponding parameters par_i. After the training the NN can be used as an approximation of the inverse function $par_i' = \varphi(F(u))$.

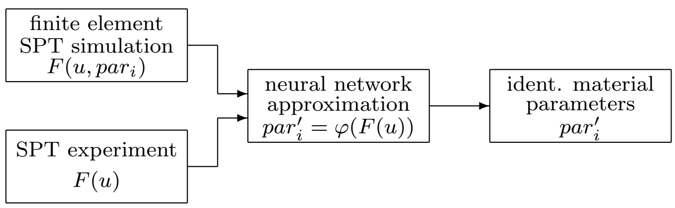

Figure 5: Scheme of the parameter identification with an inverse function (case I)

Case II: The second possibility is an optimization procedure as shown in Fig. 6. A data base is calculated as described above and used to train a NN, whereby the material parameters par_i and the punch displacement u serve as input and the corresponding punch force F as output, respectively. These NNs are an approximation for the direct problem and can be used instead of a FE-calculation. An experimental LDC is compared with the answer $F'(u)$ from the NN for an initially given parameter set. By the optimization procedure the parameters are changed in such a way, that the error $E = \| F(u) - F'(u)|_{par_i'} \|$ becomes a minimum. The optimization algorithm used here is based on Brents [18] algorithm for minimization without derivatives. It should be pointed out that common optimization techniques need a FE-calculation of the SPT for each step, which is now done very efficiently by the NN.

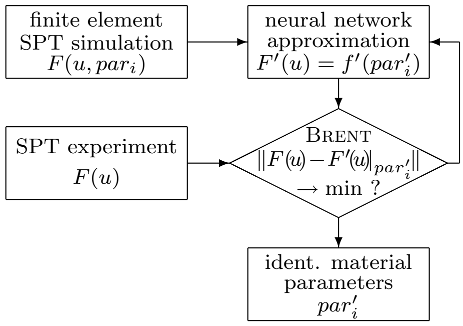

Figure 6: Scheme of the parameter identification using the direct function and the conjugate directions algorithm (case II)

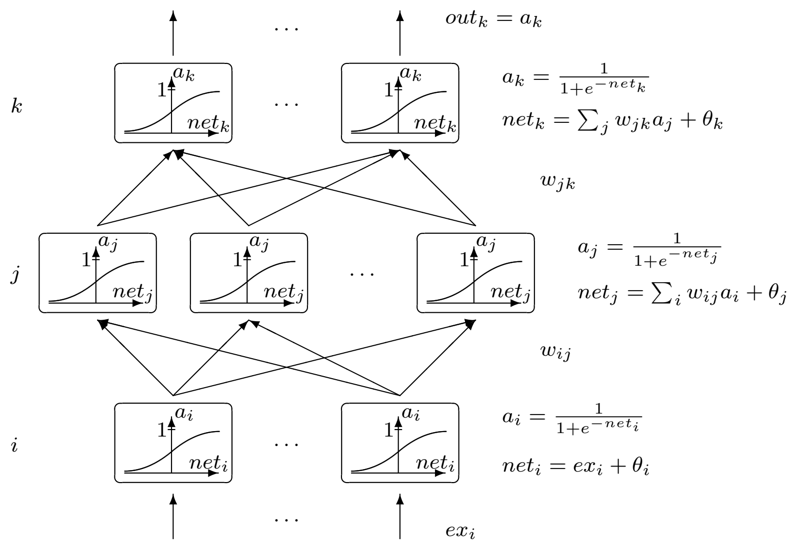

Figure 7: Scheme of a multi-layer perceptron

The NNs that are used here [19] belong to the class of multi-layer perceptrons. They contain three layers of neurons (or units) each having an activation function

$$a_i = \frac{1}{1 + e^{-net_i}} \tag{6}$$

where net_i denotes the input for unit i. All units of the input layer i get an external input ex_i, which represents in our case the discretisized and normalized load displacement curve (case I) or the vector of the normalized material parameters and the normalized punch displacement (case II). The accumulated and with ω_{ij} weighted activations a_i serve as input for the second (hidden) layer j.

$$net_j = \sum_i \omega_{ij} a_i + \theta_j \tag{7}$$

The input for the third (output) layer k comes via the weights ω_{jk} from the hidden layer. The output out_k finally represents the normalized values of the material parameters par_k (case I) or the normalized punch force (case II). Normalization is done for the input units with

$$ex_i = (par_i - par_i^{min}) \frac{ex^{max} - ex^{min}}{par_i^{max} - par_i^{min}} + ex^{min} \tag{8}$$

and for the output units with

$$out_i = (par_i - par_i^{min}) \frac{out^{max} - out^{min}}{par_i^{max} - par_i^{min}} + out^{min} \tag{9}$$

where $ex^{min} = 0.0$, $ex^{max} = 1.0$, $out^{min} = 0.1$, $out^{max} = 0.9$.

During a training procedure the weights between the layers are changed by an appropriate training algorithm. Two of them, the scaled conjugate gradient (scg) and the classical back-propagation (bprop) algorithm [19] have been tested (see Tab. 3). To check the accuracy of a NN for unknown data, validation data sets are used, which contain randomly selected subsets of the simulated data and were not part of the training patterns.

ident. case	net	no. of neurons		
		input	hidden	output
I	A	51	25	3
	B	51	25	4
II	C	4	100	1
	D	5	100	1

Table 2: Size of the NNs used for the different identification tasks

5 Results and Conclusion

Tab. 3 gives an overview about the training of the different networks. Obviously, for case I the accuracy for the approximation is much poorer than for case II. This is due to the fact that different parameter sets can lead to quite similar LDCs. This problem does not occur for case II, where the approximations of the direct FE-solution is very precise.

The identified hardening parameters for the three different materials are listed in Tab. 4. As shown in Fig. 8, FE-simulations using the identified parameters fit the experiments very well up to that point, where damage occurs.

ident. case	net	material model	training			validation		
			no. of patt.	MSE $[10^{-6}]$		no. of patt.	MSE $[10^{-6}]$	
				scg	bprop		scg	bprop
I	A	a	1321	8850	7310	10	9250	8650
		b	1321	19350	17520	10	22410	26320
	B	c	1286	43170	44630	10	70460	66030
II	C	a	67781	240	20	100	290	20
		b	67781	300	110	100	410	120
	D	c	65996	150	20	100	190	10

Table 3: Number of patterns and the mean square error after 1000 cycles for training and validation of the used networks

ident. case	net	material model	specimen	parameter			
				ε_{py}	σ^*	R_e	n
II	C	a	18Ch2MFA-017	-	1030	652	7.64
II	D	c	StE690-008	0.0102	1140	696	11.1
II	D	c	GGG40-024	0.0129	532	264	11.6

Table 4: Identified parameters for the different materials ([σ^*, R_e]=MPa)

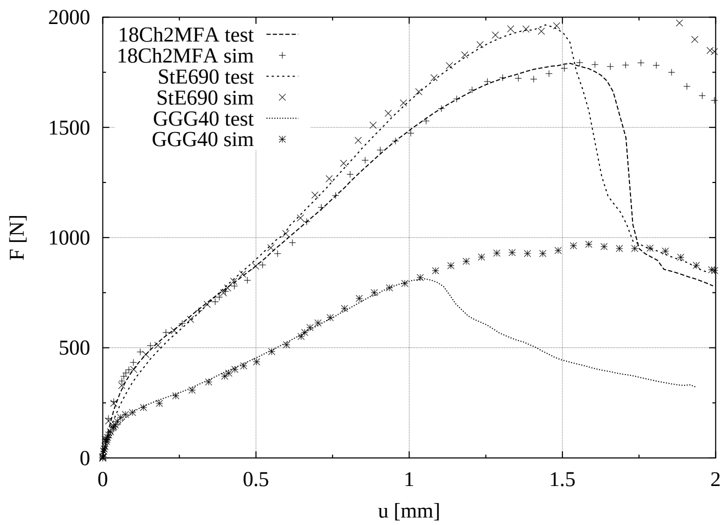

Figure 8: Experimental and simulated load displacement curves of the SPT

Using the parameters from Tab. 4, notched tensile tests have been simulated for the materials 18Ch2MFA and StE-690. Even here, the simulations predict the behavior of the experiments reasonably well (see Fig. 8) up to the point, where damage plays an important role.

In general it was found that the identification strategy (case II) using the direct approximation of the FE-solution leads to better results, than the strategy using an inverse approximation.

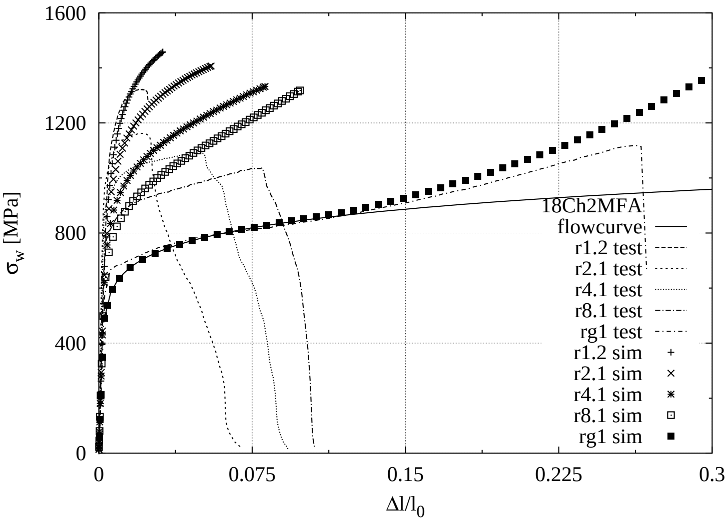

Figure 9: Experimental and simulated tensile tests of notched specimen for the material 18Ch2MFA

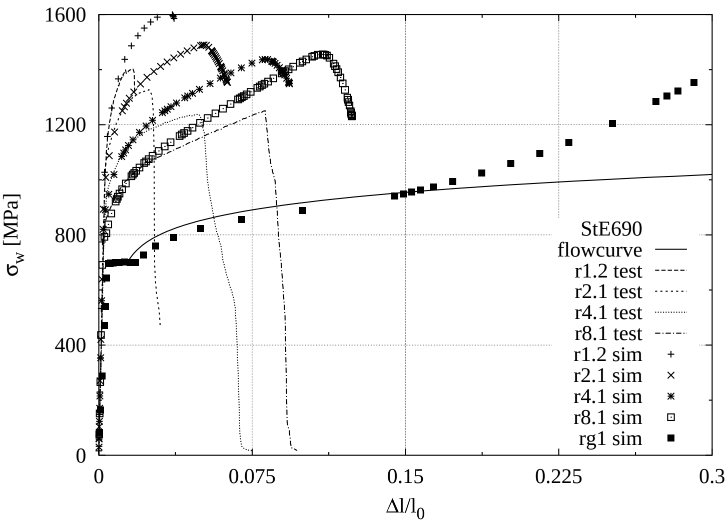

Figure 10: Experimental and simulated tensile tests of notched specimen for the material StE-690

Looking back to Fig. 8, one can found that not all information of the LDC of the SPT have been used. Especially the part where the load decreases can be used to identify parameters of the damage model, that has been mentioned earlier.

Acknowledgment

This work was gratefully funded by the German Research Foundation (DFG).

References

[1] J. Foulds, C. Jewett, L. Bisbee, T. Gabel, R. Viswanathan, In-service steam turbine rotor material evaluation by small punch testing, Steam Turbine-Generator Developments for the Power Generation Industry American Society of Mechanical Engineers, Power Division (Publication) PWR, Publ by ASME 18 (1992) 151–157.

[2] S. Jitsukawa, M. Kizaki, A. Umino, K. Shiba, A. Hishinuma, Methods and devices for small specimen testing at the Japan atomic energy research institute, ASTM Special Technical Publication. Publ by ASTM 1204 (1993) 289–307.

[3] M. Manahan, A. Argon, O. Harling, The development of a miniaturized disc bend test for the determination od postirradiation mechanical properties, Journal of Nuclear Materials 103–104 (ggf. Teil B) (1981) 1545–1550.

[4] J.-M. Baik, J. Kameda, O. Buck, Small Punch Test evaluation of intergranular embrittlement of an alloy steel, Scripta Metallurgica 17 (1983) 1443–1447.

[5] E. Fleury, J. Ha, Small punch tests to estimate the mechanical properties of steels for steam power plant: I.Mechanical strength, International Journal of Pressure Vessels and Piping 75 (9) (1998) 699–706.

[6] C. Sainte Catherine, J. Messier, C. Poussard, S. Rosinski, J. Foulds, Small Punch Test: EPRI-CEA Finite Element Simulation Benchmark an Inverse Method for the Estimation of Elastic Plastic Behavior, in: Small Specimens Test Techniques, Vol. 4, 2002, pp. 350–370.

[7] J. Bulloch, Toughness losses in low alloy steels at high temperatures: an appraisal of certain factors concerning the small punch test, International Journal of Pressure Vessels and Piping 75 (11) (1998) 791–804.

[8] X. Mao, H. Takahashi, T. Kodaira, Estimation of mechanical properties of irradiated nuclear pressure vessel steel by use of subsized ct specimen and small punch specimen, Scr Metall Mater 25 (11) (1991) 2487–2490.

[9] X. Mao, M. Saito, H. Takahashi, Small punch test to predict ductile fracture toughness J_{IC} and brittle fracture toughness K_{IC}, Scr Metall Mater 25 (11) (2000) 2481–2485.

[10] N. Huber, A. Konstantinidis, C. Tsakmakis, Determination of Poisson's ratio by spherical indentation using neural networks, Part I+II, Journal of Applied Mechanics 68 (2001) 218–229.

[11] M. Abendroth, M. Kuna, Determination of deformation and failure properties of ductile materials by means of the small punch test and neural networks, in: Proceedings of the IWCMM 12, 2002.

[12] M. Abendroth, M. Kuna, Bestimmung von Verformungs- und Versagenseigenschaften aus dem Small Punch Test, in: DVM-Bericht 235, Fortschritte der Bruch- und Schädigungsmechanik, 2003, pp. 269–278.

[13] P. W. Bridgman, Studies in Large Plastic Flow and Fracture, McGraw-Hill Book Company Inc., New York, Toronto, London, 1952.

[14] A. L. Gurson, Continuum theory of ductile rupture by void nucleation and growth: Part I – Yield criteria and flow rules for porous ductile materials, Journal of Engineering Materials and Technology 99 (1977) 2–15.

[15] V. Tvergaard, Influence of Voids on Shear Band Instabilities under Plane Strain Conditions, International Journal of Fracture Mechanics 17 (1981) 389–407.

[16] U. Mühlich, W. Brocks, T. Siegmund, A user-material subroutine of the gurson-tveergard-needleman model of porous metal plasticity for rate and temperature dependent hardening, Technical note gkss/wmg/98/1, GKSS-Forschungszentrum Geesthacht (1998).

[17] A. Franklin, Comparison between a quantitative microscope and chemical methods for assessment of non-metallic inclusions, Journal of the Iron and Steel Institute (1969) 181–186.

[18] R. P. Brent, Algorithms for Minimization Without Derivatives, Prentice-Hall, Englewood Cliffs, N.J., 1973.

[19] A. Zell, at. al., SNNS Stuttgart Neural Network Simulator, User Manual, Version 4.1 (1995).